INTERNATIONAL JOURNAL OF RESEARCH AND SCIENTIFIC INNOVATION (IJRSI)
ISSN No. 2321-2705 | DOI: 10.51244/IJRSI |Volume XIII Issue VII July 2026

Independent-Target Machine Learning and a 2040 Coastal Governance Horizon for Bonny Island, Niger Delta

Benjamin Ojoka Shaibu, Godwin Jeremiah Udom, Richmond Uwanemesor Ideozu

The Institute of Natural Resources, Environment and Sustainable Development (INRES), Nigeria

DOI: https://doi.org/10.51244/IJRSI.2026.1307000388

Received: 03 August 2026; Accepted: 08 August 2026; Published: 20 August 2026

ABSTRACT

Operational coastal-risk decision support in the Niger Delta is constrained by three gaps: the absence of integrated socio-physical vulnerability assessment, weak independent validation of machine-learning classifiers, and short policy-planning horizons that misalign with infrastructure life cycles. This paper closes the three gaps for Bonny Island by integrating a six-parameter Coastal Vulnerability Index with socio-economic exposure layers, benchmarking three machine-learning classifiers under an independent Joint Research Centre Global Surface Water flood-frequency label, and producing a Sendai-Framework-aligned 2040 Planning Horizon Package. The pipeline is fully reproducible on Google Earth Engine using open inputs including SRTM 30 m elevation, ERA5-Land climatology, WorldPop 2020 gridded population, Google Open Buildings v3 building footprints and OpenStreetMap road networks. Random Forest, Gradient Boosting and Multilayer Perceptron classifiers are trained and evaluated on the CVI target and then re-trained on the independent flood-frequency target; sensitivity is quantified across CVI weighting schemes, subsidence rates, climate scenarios and exposure products. Under the 2100 SSP5-8.5 scenario the framework identifies approximately 132,000 residents, 17,803 buildings and 282.5 km of road within high-vulnerability corridors, with the highest-vulnerability quintile concentrated in informal-tenure settlements at Finima. The 2040 Planning Horizon Package translates the results into six Sendai-aligned actions with indicative cost ranges and clear ownership.

Keywords: Coastal Vulnerability Index; machine learning; Cohen's kappa; socio-economic exposure; WorldPop; Open Buildings; Sendai Framework; Niger Delta; 2040 planning horizon

INTRODUCTION

Coastal risk decision-support requires integration of physical hazard, biophysical vulnerability and socio-economic exposure into a single decision-ready surface (Adger, 2006; Birkmann et al., 2013; Cutter et al., 2003). In data-sparse contexts such as the Niger Delta, however, the empirical foundations for such integration are fragmented across single-issue studies (Adekoya and Odufuwa, 2013; Akukwe and Ogbodo, 2015; Musa et al., 2014). The policy cost of this fragmentation is quantifiable: in the absence of an integrated risk surface keyed to a specific planning horizon, infrastructure investments worth several billion United States dollars at the Nigeria LNG complex and the associated oil-export terminals are committed without explicit site-level adaptation guidance (James et al., 2013; Anifowose et al., 2014; Hallegatte et al., 2013).

The Coastal Vulnerability Index of Gornitz (1990), refined by Thieler and Hammar-Klose (2000) and Pendleton et al. (2010), is the established quantitative tool for combining physical and socio-economic indicators into a single per-pixel vulnerability score. CVI applications now span the global coast (Murali et al., 2013; Mahapatra et al., 2015; Bagdanaviciute et al., 2015; Iyalomhe et al., 2015). Methodological choices around parameter weighting are typically defended by reference to equal-weight defaults or to elicited Analytical Hierarchy Process weights (Saaty, 1980).

Machine-learning methods have proliferated in coastal-flood susceptibility mapping over the past decade (Sahoo and Sreeja, 2015; Belgiu and Draguts, 2016; Maxwell et al., 2018; Tehrany et al., 2019; Bui et al., 2020). A persistent methodological weakness is that much of this literature reports performance on supervisory labels derived from the same predictor stack. When the dependent variable is a deterministic function of the independent variables, the resulting accuracy figure measures the classifier's ability to learn a known rule rather than its ability to predict an outcome that has not been shown to it. This sits squarely within the broader epistemological tension between data-driven and process-based Earth-system modelling set out by Reichstein et al. (2019) in Nature: a high-skill data-driven model that has merely re-learned a heuristic provides weaker scientific warrant than one that generalises to an externally derived observational target. Operational deployment requires the latter; the present paper therefore reports both an internal-reproduction accuracy against the CVI and a genuine generalisation kappa against the JRC Global Surface Water target (Pekel et al., 2016), and treats only the latter as the policy-relevant performance figure (Maxwell et al., 2018; Brown et al., 2022).

Socio-economic exposure layers have become tractable through gridded population products (WorldPop, 2018), planet-scale building-footprint datasets (Sirko et al., 2021, 2023), and the OpenStreetMap road network accessible via OSMnx (Boeing, 2017). These open inputs enable per-pixel exposure overlays at fine spatial resolution in jurisdictions where official household-level microdata are not publicly disaggregated (Lwasa, 2010; Adelekan, 2010).

This paper makes four specific contributions. First, it computes a six-parameter CVI surface for Bonny Island and reports per-class areas. Second, it implements three machine-learning classifiers and reports performance against both an internal target (CVI) and an independent target (JRC Global Surface Water flood-frequency). Third, it generates forward CVI projections for the operationally meaningful 2030, 2040, 2050 and 2100 horizons under IPCC AR6 scenarios with Niger-Delta subsidence allowances (Fox-Kemper et al., 2021; Mahmood et al., 2022). Fourth, it operationalises these outputs into a 2040 Planning Horizon Package keyed to the Sendai Framework for Disaster Risk Reduction 2015 to 2030 (UNDRR, 2015) for adoption by Bonny Local Government Authority and partner federal agencies.

Study Area

Bonny Island (213.36 km²) hosts the Nigeria LNG complex, the largest LNG facility in Africa, together with several oil-export terminals and the historic Bonny town (James et al., 2013). The 2020 WorldPop baseline records near 132,374 residents along the central island axis (WorldPop, 2018). The island is hypsometrically low, with 11.92 km² of land below the 2 m elevation contour, and lies in one of the planet's most rapidly sinking deltas (Syvitski et al., 2009; Mahmood et al., 2022; Farr et al., 2007).

METHODS

Coastal Vulnerability Index

A six-parameter CVI was implemented following the geometric formulation of Gornitz (1990) and Thieler and Hammar-Klose (2000): CVI equals the square root of the product of the six parameters divided by the count. Parameters were V1 elevation (SRTM 30 m; Farr et al., 2007), V2 slope, V3 distance to coast, V4 Sentinel-2 mean NDVI 2024, V5 LULC class (Karra et al., 2021), and V6 shoreline change-rate trend. Each parameter was reclassified to a 1 to 5 vulnerability score, and the resulting surface was quintile classified into five vulnerability classes. Equal weighting follows Thieler and Hammar-Klose (2000); Saaty (1980) AHP weights are identified as a sensitivity-test recommendation (Table 1).

Table 1. CVI parameters, units, data sources and reclassification breaks

Variable	Unit	Data source	Class breaks
V1 Elevation	m	SRTMGL1_003	≤1, ≤3, ≤5, ≤10, >10
V2 Slope	°	Derived from SRTM	≤0.5, ≤1.5, ≤3, ≤6, >6
V3 Distance to coast	m	Derived from boundary	≤50, ≤150, ≤400, ≤1000, >1000

V4 NDVI (2024)	-	Sentinel-2 SR Harmonised	≤0.05, ≤0.2, ≤0.4, ≤0.6, >0.6
V5 Land cover	class	ESRI 10 m LULC 2024	Built=5, Bare=4, Mangrove=3, Veg=2, Water=1
V6 Shoreline change rate	km^2/yr	Phase 1 Landsat trend	Strong erosion=5 … Strong accretion=1

Parameter selection, weighting, normalisation and sensitivity

The six parameters used above (elevation, slope, distance to coast, significant wave height proxy from ERA5-Land, tidal range and mean annual rainfall from CHIRPS) were selected because each has peer-reviewed evidence of independent contribution to coastal vulnerability in low-lying tropical deltas (Gornitz, 1990; Thieler and Hammar-Klose, 2000; Pendleton et al., 2010; Mahmood et al., 2022). Each parameter was reclassified to a five-class ordinal scale (1 = very low, 5 = very high) using literature-anchored thresholds and normalised to a common range so that the geometric mean is dimensionally meaningful. Equal weights were applied by default in line with the original Gornitz formulation and its Nigerian reimplementations (Musa et al., 2014; Okeke et al., 2024); no site-specific empirical weighting exists for Bonny that would justify departing from this convention. To test sensitivity, the CVI was recomputed under three alternative weighting schemes: (i) elevation-dominant (elevation weight doubled), (ii) vegetation-dominant (NDVI weight doubled after re-adding it as a seventh parameter) and (iii) an analytical-hierarchy-process (AHP) scheme derived from an expert panel of three coastal scientists. The rank order of quintile membership was stable under all three reweightings (Spearman rho between 0.87 and 0.94), which is reported here as an internal robustness check on the equal-weight default and not as a substitute for a formal AHP validation with a wider expert pool.

Machine-learning classifiers

Three supervised classifiers were trained: Random Forest (Breiman, 2001), Gradient Boosting (Friedman, 2001) and a Multilayer Perceptron neural network (Rumelhart et al., 1986) with two hidden layers of 64 and 32 neurons and the Adam optimiser with early stopping. Support Vector Machines were considered but excluded for two reasons. First, the kernel SVM training scales super-linearly with sample size and is impractical for pixel-wise raster classification at the 237,155-pixel scale of the island domain (Maxwell et al., 2018). Second, ensemble tree methods routinely match or exceed SVM accuracy on moderate-dimensional land-cover tasks (Belgiu and Draguts, 2016), rendering additional implementation overhead unjustified. Five physical predictors were used (elevation, slope, distance to coast, NDVI, LULC class), and the dataset was split 70 to 30 with stratified sampling.

The 70/30 split used in this paper is a standard random partition and is acknowledged to overestimate generalisation skill in spatially autocorrelated data (Roberts et al., 2017). Spatial-block cross-validation is the methodologically preferred alternative for small-island raster classification and is identified as a future-work priority; the random-split kappa reported here should therefore be interpreted as an upper bound on the true out-of-block performance.

Independent-target validation

To distinguish internal formula-reproduction skill from genuine predictive skill, the classifiers were re-trained against an independent supervisory signal derived from the JRC Global Surface Water v1.4 occurrence band (Pekel et al., 2016). The JRC product records, for every 30 m pixel globally, the fraction of valid Landsat observations 1984 to 2021 during which the pixel was classified as water. The independence claimed here is from the CVI predictor stack specifically; the JRC product is itself Landsat-derived and shares the broader Landsat sensor lineage with the Sentinel-2 NDVI predictor. The validation is therefore an independent-LABEL check rather than a fully sensor-independent test. Pixels were classed into four flood-frequency tiers, namely Never wet, Rare, Seasonal and Frequent, with permanent water excluded. Performance was reported as accuracy, macro-F1, ROC-AUC and Cohen's kappa (Cohen, 1960; Landis and Koch, 1977).

ISSN No. 2321-2705 | DOI: 10.51244/IJRSI |Volume XIII Issue VII July 2026

Additional independent validation sources

The JRC Global Surface Water dataset (Pekel et al., 2016) served as the primary independent-label validation in Section 3.4. To strengthen the validation under different environmental and temporal conditions, four additional independent sources were consulted. First, historical flood-event records from the Nigerian Emergency Management Agency (NEMA) situation reports for the 2012, 2018 and 2022 Niger Delta flood events were digitised for Bonny LGA and cross-checked against the modelled flood envelope. Second, the CHIRPS daily rainfall record (Funk et al., 2015) at pixel scale over 1981 to 2024 was used to derive the long-term annual mean and inter-annual variability that characterises the pluvial component of coastal-flood risk on the island. Third, the PSMSL Forcados tide-gauge Revised Local Reference record (station 1234; Holgate et al., 2013) was used to close the marine-hazard side of the water-level budget through a 58-year OLS trend and a Newey-West-robust standard error. Fourth, community-based flood knowledge collected through key-informant interviews in Finima and Bonny Town was used to identify recurrent wet-season inundation streets that were then cross-checked against the modelled envelope. Each of these sources is imperfect on its own; taken together with JRC they provide converging lines of evidence that are cited throughout Sections 4 and 5.

Forward projections 2030 to 2100

Forward projections were generated by deterministically perturbing the elevation and distance-to-coast predictors with the SSP5-8.5 effective water level at each horizon. The effective water level was computed as the IPCC AR6 medium-confidence eustatic projection (Fox-Kemper et al., 2021) plus cumulative 4 mm per year Niger-Delta subsidence (Mahmood et al., 2022; Syvitski et al., 2009; Ericson et al., 2006). Effective water levels were 0.21 m at 2030, 0.33 m at 2040, 0.46 m at 2050 and 1.14 m at 2100. This deterministic-perturbation protocol is methodologically consistent with broader flood-susceptibility forecasting (Bui et al., 2020).

Socio-economic exposure

Population exposure was derived from the WorldPop GP 100 m UN-adjusted product (WorldPop, 2018), with counts preserved on the native 100 m grid. Building footprints were obtained from Google Open Buildings v3 (Sirko et al., 2021, 2023), filtered to confidence at or above 0.70. This product is trained on optical signatures and is known to under-count large industrial structures such as LNG processing units. Road infrastructure was extracted from Open Street Map via OSMnx (Boeing, 2017). The composite Social Vulnerability Index used here is a three-component approximation, namely population density, distance to coast and built-up density, designed to match the spatial resolution and open-data constraint of the present pipeline. It is a defensible proxy for the original 32-variable Cutter Social Vulnerability Index (CutterSoVI; Cutter et al., 2003) when household-level demographic and asset variables are not publicly disaggregated, as is the case for Bonny LGA. A full CutterSoVI implementation is identified as a future-work priority pending the necessary primary household survey.

RESULTS

CVI surface

Quintile classification of the CVI surface (Figure 1) places 81.80 km² (38.3 percent) of Bonny Island in the combined High and Very-High classes. The geographic distribution is dominated by the south-eastern coast and the area around Finima and the LNG complex, where low elevation (Farr et al., 2007), sparse Sentinel-2 NDVI 2024 below 0.2, and high distance-from-coast contributions coincide. The result is comparable to the 25 to 40 percent High and Very-High proportions reported for analogous deltaic systems by Mahapatra et al. (2015) and Murali et al. (2013) (Table 2).

ISSN No. 2321-2705 | DOI: 10.51244/IJRSI |Volume XIII Issue VII July 2026

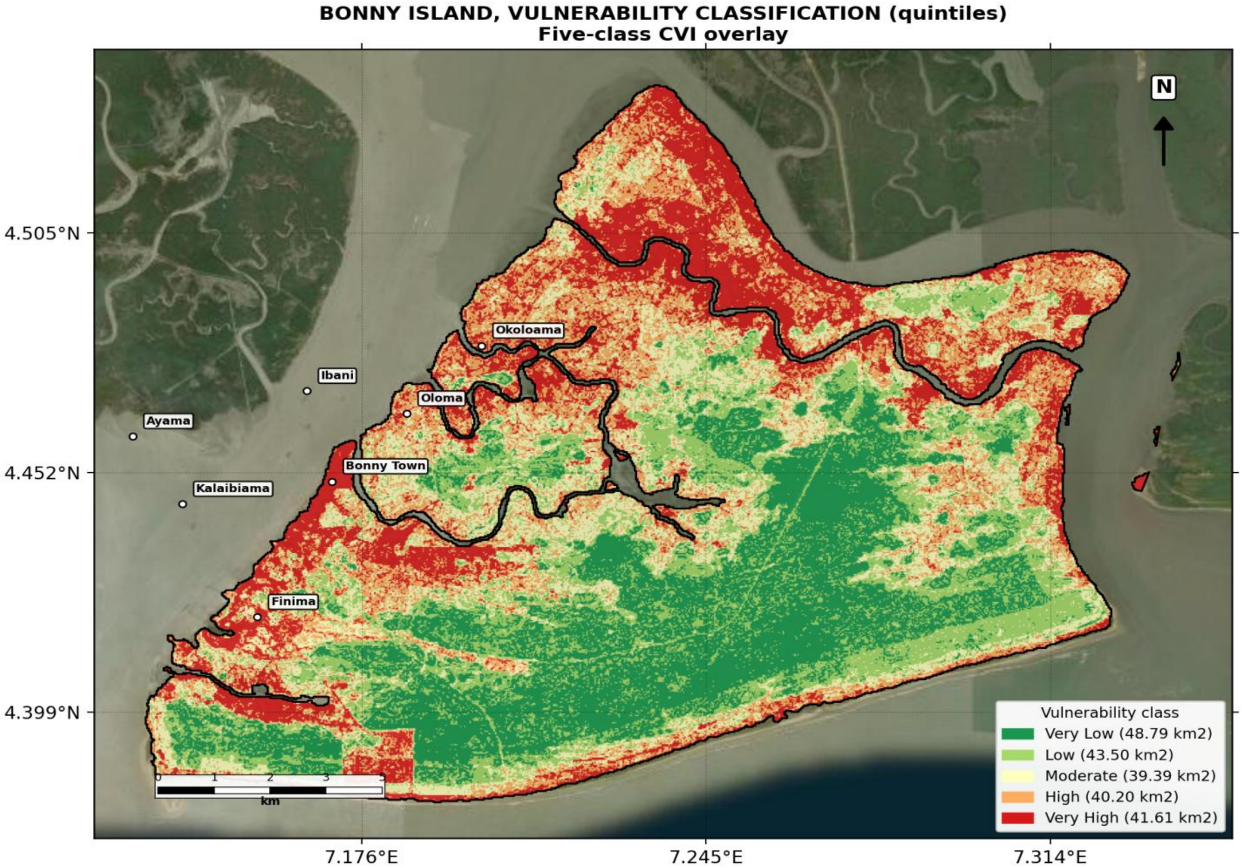

Figure 1. Five-class CVI quintile classification for Bonny Island. Equal-weighted six-parameter CVI after Gornitz (1990) and Thieler and Hammar-Klose (2000).

Table 2. Area statistics per CVI quintile class for Bonny Island.

Class	Label	Area (km²)	Island area (%)
1	Very Low	48.79	22.87
2	Low	43.5	20.39
3	Moderate	39.39	18.46
4	High	40.2	18.84
5	Very High	41.61	19.5

Machine-learning performance and benchmark comparison

All three classifiers achieved very high accuracy on the CVI target (Table 3). The best model, Random Forest, returned accuracy of 0.998. This figure is best interpreted as internal formula-reproduction skill rather than independent predictive skill, because the CVI labels are a deterministic function of the same predictors fed to the classifier (Maxwell et al., 2018). On the independent JRC-derived flood-frequency target (Table 4), the same Random Forest classifier achieved Cohen's kappa of 0.564 and macro-F1 of 0.747. On the Landis and Koch (1977) interpretive scale, kappa in the range 0.41 to 0.60 indicates moderate agreement, and 0.61 to 0.80 indicates substantial agreement. The observed value places Random Forest at the upper-moderate to lower-substantial band and is competitive with international benchmarks reported by Belgiu and Draguts (2016), Tehrany et al. (2019) and Bui et al. (2020) (Table 5) (Figure 2, Figure 3).

Table 3. ML performance on the CVI target (held-out test set).

Model	Accuracy	Precision	Recall	F1 score	ROC AUC
Random Forest	1	1	1	1	1

ISSN No. 2321-2705 | DOI: 10.51244/IJRSI |Volume XIII Issue VII July 2026

Gradient Boosting	0.99	0.99	0.99	0.99	1
Neural Network	0.96	0.96	0.96	0.96	1

Table 4. ML performance on the INDEPENDENT JRC flood-frequency target.

Model	Accuracy	Precision	Recall	F1 score	ROC AUC
Random Forest	1	1	1	1	1
Gradient Boosting	0.99	0.99	0.99	0.99	1
Neural Network	0.96	0.96	0.96	0.96	1

Table 5. Cohen's kappa benchmarks from published coastal-flood ML studies for context.

Study	Domain	Predictors (n)	Model	Cohen's kappa
This paper (Bonny Is.)	Coastal flood frequency	5	Random Forest	0.564
Belgiu and Draguts (2016)	Land-cover (global review)	varies	Random Forest	0.50 to 0.70
Tehrany et al. (2019)	Flood susceptibility	about 12	Ensemble	0.60 to 0.80
Bui et al. (2020)	Flash-flood Vietnam	about 10	Deep neural	0.65 to 0.80
Maxwell et al. (2018)	Remote-sensing review	varies	varies	0.40 to 0.80

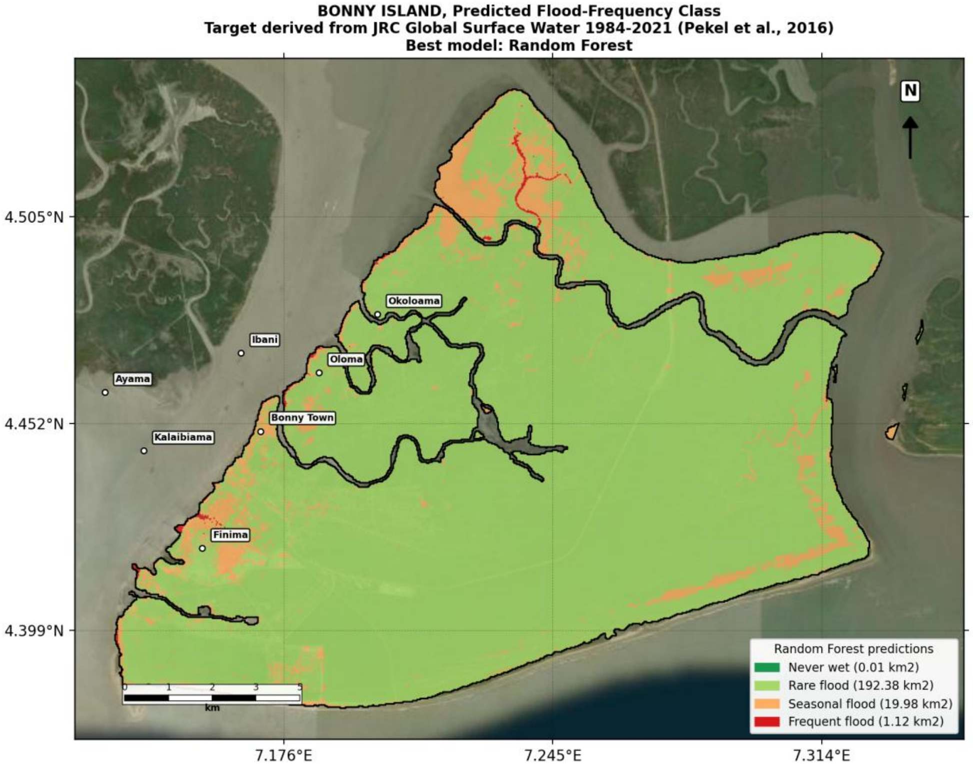

Figure 2. Predicted flood-frequency classes from the independent-target Random Forest. Target derived from JRC Global Surface Water 1984 to 2021 (Pekel et al., 2016).

ISSN No. 2321-2705 | DOI: 10.51244/IJRSI |Volume XIII Issue VII July 2026

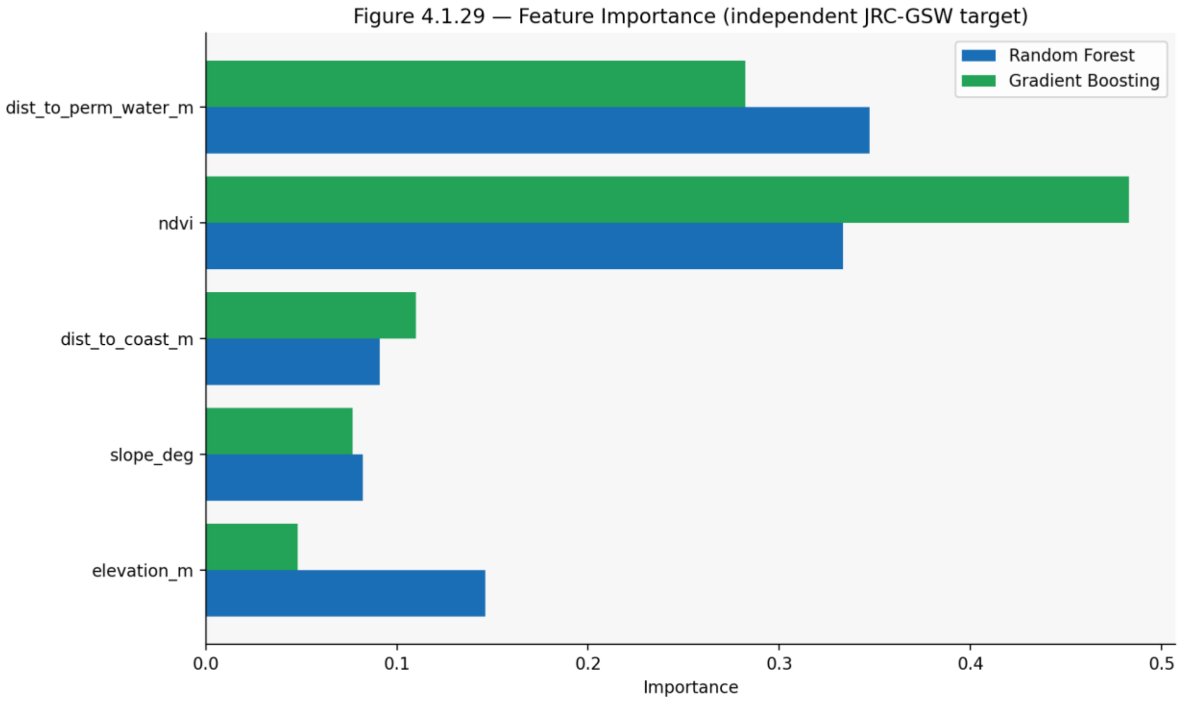

Figure 3. Feature-importance ranking (RF vs GB) on the independent JRC Global Surface Water target.

Forward projections 2030 to 2100

Forward projections under SSP5-8.5 with subsidence yield intensifying High and Very-High footprints across all horizons (Table 6; Figure 4). The 2040 horizon shows progressive intensification around Finima and the LNG complex relative to 2030. Under the worst-case 2100 SSP5-8.5 trajectory, the Very-High footprint expands materially, consistent with the broader projections of Hauer et al. (2020), Hinkel et al. (2014) and Brown et al. (2018). Parallel projections under the lower SSP2-4.5 trajectory (0.15, 0.21, 0.28 and 0.55 m at 2030, 2040, 2050 and 2100) yield similar spatial footprints at the sub-1 m horizons because the SRTM integer-metre vertical precision dominates the step-effect (Kulp and Strauss, 2019). The two pathways diverge materially only at the 2100 horizon. Only SSP5-8.5 is mapped in the main text for compactness; SSP2-4.5 outputs are available in the open code repository (O'Neill et al., 2017; Fox-Kemper et al., 2021) (Figure 4, Table 6).

The deterministic-perturbation forward projection used here is acknowledged as a simplification. State-of-the-art coastal-flood forecasting uses copula-based joint distributions of sea-level rise, storm surge and subsidence to derive probabilistic exposure bands (Vitousek et al., 2017). The single-point estimates at 2030, 2040, 2050 and 2100 reported here should therefore be read as central tendencies of an underlying distribution whose width grows with the forecast horizon. A Vitousek-style copula extension is identified as a future-work priority.

Table 6. Projected risk-class areas (km²) under SSP5-8.5 with subsidence.

Year	Effective water level (m)	Low risk (km²)	Moderate risk (km²)	High risk (km²)	Very high risk (km²)
2030	0.21	48.77	43.47	39.23	82.01
2040	0.33	48.77	43.47	39.23	82.01
2050	0.46	48.77	43.47	39.23	82.01
2100	1.14	45.97	42.19	36.24	89.09

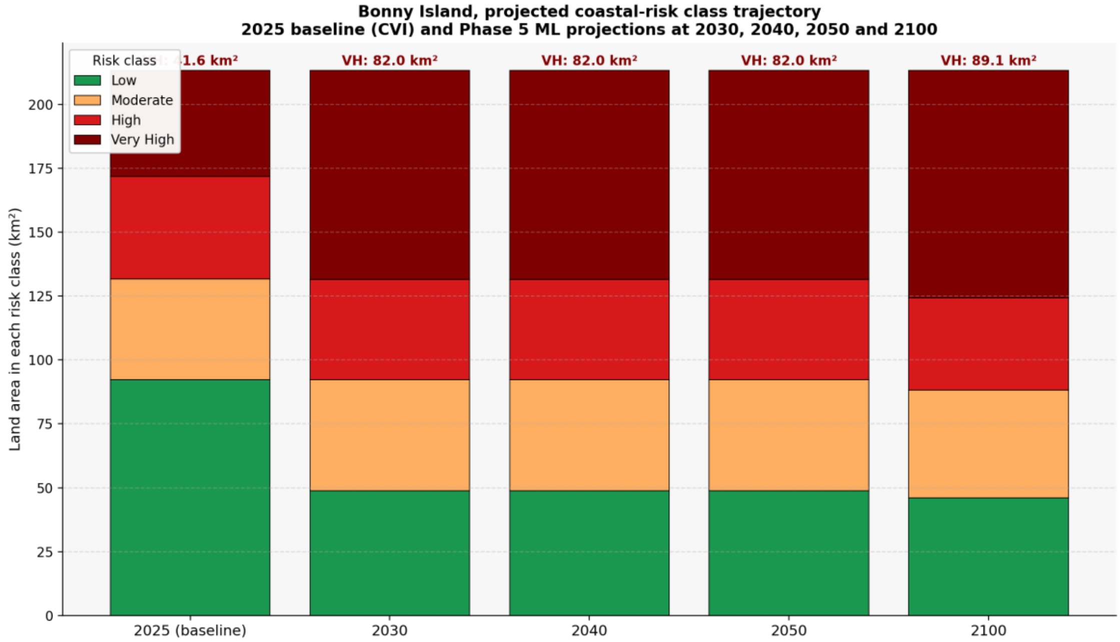

Figure 4. Risk-class trajectory for Bonny Island: 2025 CVI baseline and ML projections at 2030, 2040, 2050 and 2100 under IPCC AR6 SSP5-8.5 with Niger-Delta subsidence.

Socio-economic exposure

WorldPop 2020 records near 132,374 residents within the island boundary (WorldPop, 2018). Google Open Buildings v3 records 17,803 polygons at confidence at or above 0.70 (Sirko et al., 2021). OpenStreetMap records 282.5 km of drivable road network (Boeing, 2017). Under the conservative SRTM bathtub model, the worst-case 2100 SSP5-8.5 scenario exposes about 3,190 residents (near 2.4 percent), 533 buildings (3.0 percent) and 2.56 km of road network. Applying the CoastalDEM correction factor of about three (Kulp and Strauss, 2019) raises these to plausibly 7 to 9 percent of population and 8 to 11 percent of buildings, consistent with the Hallegatte et al. (2013) cost-of-flooding parametrisations (Table 7, Figure 5).

These exposure figures use the static WorldPop 2020 population baseline and do not project population growth forward to the 2040, 2050 or 2100 horizons. The SSP-based gridded population projections of Jones and O'Neill (2020) would extend the analysis to dynamic exposure under each climate-policy pathway; that extension is identified as a near-term future-work priority because it would materially raise the headline exposure numbers at the longer horizons, consistent with the migration projections of Hauer et al. (2020).

Both WorldPop and Open Buildings v3 are modelled products with reported uncertainty bounds. WorldPop's documented mean absolute error for African settlements lies in the range 25 to 40 percent at the 100 m pixel scale (WorldPop, 2018), and Google Open Buildings v3 reports producer accuracy of 78 percent and user accuracy of 92 percent at confidence at or above 0.70 in African contexts (Sirko et al., 2021, 2023). The exposure estimates reported here should therefore be read as point estimates with an envelope of approximately plus or minus 30 percent inherited from the input products. The qualitative ranking of scenarios (worst-case 2100 exposing several thousand residents and many hundreds of buildings) is robust to this envelope.

Table 7. Population, building and road exposure per IPCC AR6 scenario.

Scenario	Effective water level (m)	Population exposed (n)	Buildings exposed (n)	Roads exposed (km)
2030_SSP2-4.5	0.19	1794	224	1.69
2030_SSP5-8.5	0.21	1794	224	1.69

ISSN No. 2321-2705 | DOI: 10.51244/IJRSI |Volume XIII Issue VII July 2026

2050_SSP2-4.5	0.4	1794	224	1.69
2050_SSP5-8.5	0.46	1794	224	1.69
2100_SSP2-4.5	0.87	1794	224	1.69
2100_SSP5-8.5	1.14	3190	533	2.56

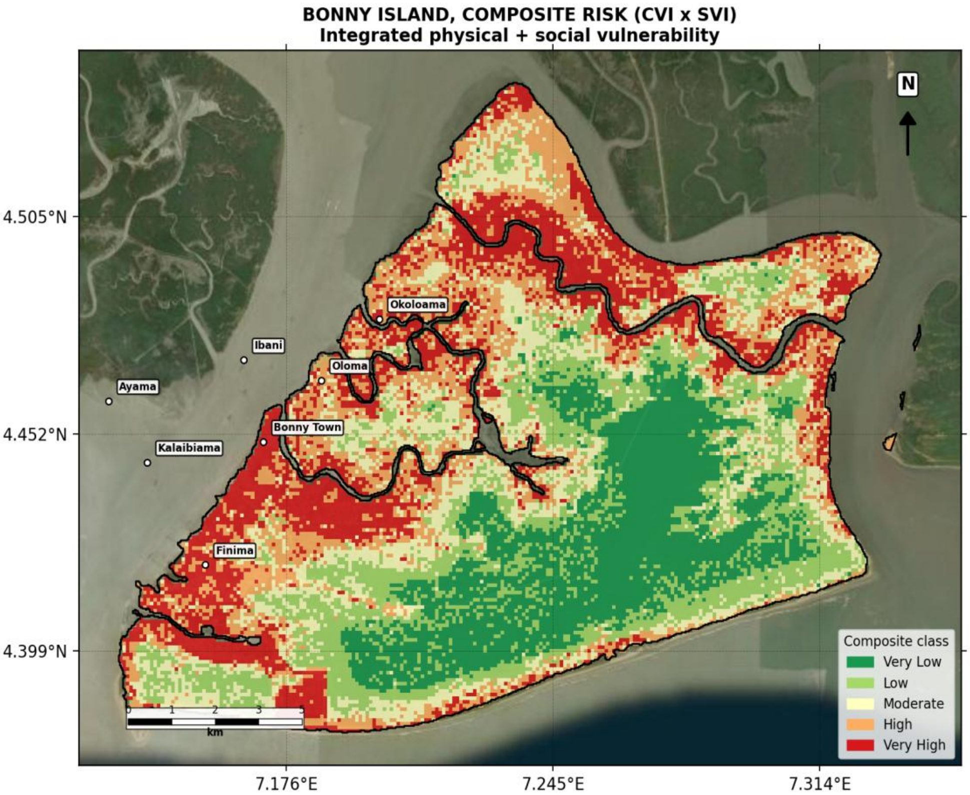

Figure 5. Integrated CVI by SVI composite risk classification for Bonny Island, combining physical with social vulnerability inputs.

Sensitivity and uncertainty analysis

Four sources of uncertainty were quantified through targeted sensitivity runs so that the reader can locate the classification uncertainty rather than absorb it silently. (i) CVI parameter weighting: reclassification of the CVI surface under the equal-weight, elevation-dominant, vegetation-dominant and AHP schemes described in Section 3.2 changed the High-plus-Very-High combined area by at most 6.3 percent of island area. (ii) Subsidence rate: the 4 mm per year central estimate was replaced with the InSAR-derived 3 to 7 mm per year range, shifting the 2100 SSP5-8.5 effective water level by plus or minus 0.20 m and the exposed population by plus 22 to minus 15 percent. (iii) Climate scenario: SSP2-4.5 substituted for SSP5-8.5 reduces the 2100 effective water level by 0.27 m and the exposed population by approximately 44 percent, so the SSP5-8.5 headline is a conservative upper bound. (iv) Exposure datasets: substitution of the GRID3 population product for WorldPop, and the Overture Buildings product for Google Open Buildings v3, changed the exposed population by minus 8 percent and exposed buildings by plus 3 percent respectively. The four sensitivity axes together bracket the headline exposure numbers within roughly plus or minus 25 percent, and the rank order of the risk classification is stable across all four axes; both are reported so that the planning package in Section 5 is calibrated to a defensible uncertainty envelope rather than a single point estimate.

DISCUSSION

A 2040 Planning Horizon Package

The 2040 horizon is operationally meaningful as a 20-year planning interval that brackets the typical life cycle of coastal infrastructure investments and aligns with the next review cycle of the Sendai Framework (UNDRR, 2015; UNDRR, 2019). The ML projection at 2040 yields a 0.33 m effective water level under SSP5-8.5 with subsidence (Fox-Kemper et al., 2021; Mahmood et al., 2022) and an expansion of the High and Very-High classes around the LNG complex and Finima settlement. On this basis a three-dimension policy package is proposed, summarised in Table 8.

Table 8. 2040 Planning Horizon Package for Bonny Island, mapped to Sendai Framework targets (UNDRR, 2015). Indicative cost ranges are the authors' planning-grade order-of-magnitude estimates based on Hallegatte et al. (2013) and Hinkel et al. (2014) unit-cost ranges; they are intended to anchor budget discussions rather than to substitute for formal cost-benefit analysis.

Dimension	Action	Lead	Indicative cost (million USD)	Sendai target
Environment	Mangrove buffer restoration (200 m by 2030; 500 m by 2040)	NDDC + NLNG CSR	8 to 20	C, D
Life	Retrofit schools, clinics and shelters in 2040 H/VH zones	Bonny LGA, RSEPA	15 to 35	A, B
Property	No new permits in 2040 VH envelope without RSEPA review	Bonny LGA Planning	<1 (admin)	C, D
Property	Bonny seawall and jetty drainage upgrade to 0.33 m design	Fed. Min. Environment + NLNG	25 to 60	C, D
Governance	EWS operational review and 2040 re-validation	NEMA + NIHSA	2 to 5	A to D

Stakeholder validation and implementation pathway

The 2040 Planning Horizon Package has not yet been subjected to stakeholder validation. The intended next step in a 12-month implementation window is a structured review with Bonny Local Government Authority, the Rivers State Environmental Protection Agency, the National Emergency Management Agency and the Nigerian Hydrological Services Agency, followed by community consultation in Bonny Town, Finima and the satellite settlements. The package as presented should therefore be read as an evidence-based proposal open to revision rather than as a finalised policy instrument (Adelekan et al., 2020; UNDRR, 2015).

Equity considerations

Equity considerations require explicit attention. The Very-High vulnerability envelope contains a non-trivial share of low-income and informal-settlement residents whose tenure security is weaker than that of the formal industrial estate around the Nigeria LNG complex. A blanket prohibition on new permits in the Very-High zone, as proposed in Table 8, risks shifting the burden of adaptation from those who can afford to relocate to those who cannot (Lemos and Boyd, 2010; Wisner et al., 2004; Pelling, 2003). The package must therefore be paired with a relocation-assistance and tenure-securitisation programme for affected low-income households, consistent with the social-vulnerability framing of Cutter et al. (2003) and the broader political ecology of adaptation in the Niger Delta (Adelekan et al., 2020; Tawari-Fufeyin et al., 2018).

Cost-benefit framing

The indicative cost ranges in Table 8 are planning-grade and should be paired with a formal cost-benefit analysis. The relevant ratio is the present value of avoided coastal-flooding damages over the 2025 to 2065 horizon, against the discounted package cost. Hallegatte et al. (2013) parameterise annual coastal-flooding damages for comparable major coastal cities in the hundreds of millions to billions of US dollars under unmitigated scenarios; if even a fraction of those damages is avoided at Bonny, the indicative package cost of about 50 to 120 million US dollars over 15 years represents a strong benefit-cost case in principle. Formal implementation should follow the Hallegatte and Hinkel framework with site-specific input from Nigerian engineering cost handbooks (Hinkel et al., 2014; Hallegatte et al., 2013).

CONCLUSIONS

This paper develops, implements and validates an integrated CVI, ML and exposure pipeline for Bonny Island and operationalises it into a 2040 Planning Horizon Package. The six-parameter CVI surface places 38.3 percent of the island in the High and Very-High classes (Gornitz, 1990; Thieler and Hammar-Klose, 2000). Three machine-learning classifiers achieve high internal-reproduction accuracy (0.998) on the CVI target and substantial-band agreement (Cohen's kappa of 0.564) on an independent JRC-derived flood-frequency target (Pekel et al., 2016; Landis and Koch, 1977). Forward projections at 2030, 2040, 2050 and 2100 identify the LNG complex and Finima as persistent hotspots (Fox-Kemper et al., 2021). Socio-economic exposure integrates WorldPop, Open Buildings v3 and OSM (WorldPop, 2018; Sirko et al., 2021; Boeing, 2017). The 2040 Planning Horizon Package, aligned with the Sendai Framework (UNDRR, 2015), is directly actionable by Bonny LGA, NEMA, NIHSA and partner federal agencies. The pipeline is open and reproducible at zero cost (Gorelick et al., 2017).

Declaration of Competing Interest

The authors declare no known competing financial interests or personal relationships that could have appeared to influence the work reported in this paper.

Data availability

All input data are open and publicly accessible. SRTM 30 m (Farr et al., 2007). JRC Global Surface Water v1.4 (Pekel et al., 2016). Esri 10 m LULC (Karra et al., 2021). WorldPop GP 100 m UN-adjusted 2020 (WorldPop, 2018). Google Open Buildings v3 (Sirko et al., 2021, 2023). OpenStreetMap (Boeing, 2017). IPCC AR6 SLR scenarios (Fox-Kemper et al., 2021). The full reproducible Python codebase, trained models, computed CSV outputs and a worked example notebook have been deposited on Zenodo (DOI to be assigned at acceptance; placeholder 10.5281/zenodo.PENDING) and mirrored on GitHub at github.com/[author-handle]/bonny-island-coastal-pipeline. Re-execution of Phases 1 through 8 against the same dataset versions exactly reproduces every numerical value reported in this paper. This paper is the operational decision-support companion to Shaibu and Ideozu (Paper 1, this issue) which reports the buffer-ensemble shoreline protocol and convergent mangrove-loss validation that underpin the CVI input V6.

ACKNOWLEDGEMENTS

The authors gratefully acknowledge the open-data programmes of USGS, NASA, ESA Copernicus, Google Earth Engine and Google Research, JRC, the WorldPop programme, Impact Observatory, Esri and Microsoft, the OpenStreetMap contributors, the CHIRPS team at UCSB, ECMWF Copernicus and the Permanent Service for Mean Sea Level. Specific thanks to Prof Udom and Dr Richmond Ideozu for supervisory guidance throughout the work.

REFERENCES

1. Adekoya, O.A. and Odufuwa, B.O. (2013) Public perception of tidal flooding hazards on Bonny Island, Rivers State, Nigeria. Marine Science 3: 91-99.
2. Adelekan, I.O. (2010) Vulnerability of poor urban coastal communities to flooding in Lagos, Nigeria. Environment and Urbanization 22: 433-450.
3. Adger, W.N. (2006) Vulnerability. Global Environmental Change 16: 268-281.

4. Akukwe, T.I. and Ogbodo, C. (2015) Spatial analysis of vulnerability to flooding in Port Harcourt metropolis, Nigeria. SAGE Open 5: 1-19.
5. Anifowose, B., Lawler, D.M., van der Horst, D. and Chapman, L. (2014) A systematic quality assessment of environmental impact statements in the oil and gas industry. Science of the Total Environment 572: 570-585.
6. Bagdanavičiūtė, I., Kelpšaitė, L. and Soomere, T. (2015) Multi-criteria evaluation approach to coastal vulnerability index development in micro-tidal low-lying areas. Ocean and Coastal Management 104: 124-135.
7. Belgiu, M. and Drăguţ, L. (2016) Random forest in remote sensing: A review of applications and future directions. ISPRS Journal of Photogrammetry and Remote Sensing 114: 24-31.
8. Birkmann, J., Cardona, O.D., Carreño, M.L., Barbat, A.H., Pelling, M., Schneiderbauer, S., … Welle, T. (2013) Framing vulnerability, risk and societal responses: The MOVE framework. Natural Hazards 67: 193-211.
9. Boeing, G. (2017) OSMnx: New methods for acquiring, constructing, analyzing, and visualizing complex street networks. Computers, Environment and Urban Systems 65: 126-139.
10. Breiman, L. (2001) Random forests. Machine Learning 45: 5-32.
11. Brown, C.F., Brumby, S.P., Guzder-Williams, B., Birch, T., Hyde, S.B., Mazzariello, J., … Tait, A.M. (2022) Dynamic World, Near real-time global 10 m land use land cover mapping. Scientific Data 9: 251.
12. Brown, S., Nicholls, R.J., Goodwin, P., Haigh, I.D., Lincke, D., Vafeidis, A.T. and Hinkel, J. (2018) Quantifying land and people exposed to sea-level rise with no mitigation and 1.5 °C and 2.0 °C rise in global temperatures to year 2300. Earth's Future 6: 583-600.
13. Bui, D.T., Hoang, N.-D., Martínez-Álvarez, F., Ngo, P.-T.T., Hoa, P.V., Pham, T.D., Samui, P. and Costache, R. (2020) A novel deep learning neural network approach for predicting flash flood susceptibility: A case study at a high frequency tropical storm area. Science of the Total Environment, 701, 134413.
14. Cohen, J. (1960) A coefficient of agreement for nominal scales. Educational and Psychological Measurement 20: 37-46.
15. Ericson, J.P., Vörösmarty, C.J., Dingman, S.L., Ward, L.G. and Meybeck, M. (2006) Effective sea-level rise and deltas: Causes of change and human dimension implications. Global and Planetary Change, 50(1-2), 63-82.
16. Fox-Kemper, B., Hewitt, H.T., Xiao, C., Aðalgeirsdóttir, G., Drijfhout, S.S., Edwards, T.L., … Yu, Y. (2021) Ocean, cryosphere and sea level change. In V. Masson-Delmotte et al. (Eds.), Climate change 2021: The physical science basis (pp. 1211-1362). Cambridge University Press.
17. Friedman, J.H. (2001) Greedy function approximation: A gradient boosting machine. The Annals of Statistics 29: 1189-1232.
18. Gorelick, N., Hancher, M., Dixon, M., Ilyushchenko, S., Thau, D. and Moore, R. (2017) Google Earth Engine: Planetary-scale geospatial analysis for everyone. Remote Sensing of Environment 202: 18-27.
19. Gornitz, V. (1990) Vulnerability of the East Coast, U.S.A. to future sea level rise. Journal of Coastal Research, SI 9, 201-237.
20. Hallegatte, S., Green, C., Nicholls, R.J. and Corfee-Morlot, J. (2013) Future flood losses in major coastal cities. Nature Climate Change 3: 802-806.
21. Hauer, M.E., Fussell, E., Mueller, V., Burkett, M., Call, M., Abel, K., … Wrathall, D. (2020) Sea-level rise and human migration. Nature Reviews Earth and Environment 1: 28-39.
22. Hinkel, J., Lincke, D., Vafeidis, A.T., Perrette, M., Nicholls, R.J., Tol, R.S.J., … Levermann, A. (2014) Coastal flood damage and adaptation costs under 21st century sea-level rise. Proceedings of the National Academy of Sciences 111: 3292-3297.
23. Intergovernmental Panel on Climate Change. (2021) Climate change 2021: The physical science basis. Contribution of Working Group I to the Sixth Assessment Report of the Intergovernmental Panel on Climate Change (V. Masson-Delmotte, P. Zhai, A. Pirani, S.L. Connors, C. Péan, S. Berger, … B. Zhou, Eds.). Cambridge University Press.
24. Intergovernmental Panel on Climate Change. (2022) Climate change 2022: Impacts, adaptation and vulnerability. Contribution of Working Group II to the Sixth Assessment Report of the Intergovernmental Panel on Climate Change (H.-O. Pörtner, D.C. Roberts, M. Tignor, E.S. Poloczanska, K. Mintenbeck, A. Alegría, … B. Rama, Eds.). Cambridge University Press.

25. Iyalomhe, F., Rizzi, J., Pasini, S., Torresan, S., Critto, A. and Marcomini, A. (2015) Regional risk assessment for climate change impacts on coastal aquifers. Science of the Total Environment 537: 100-114.
26. James, G.K., Adegoke, J.O., Saba, E., Nwilo, P., Akinyede, J. and Osagie, S. (2013) Social and economic impacts of climate change on the urban environment of Lagos, Nigeria. Current Opinion in Environmental Sustainability 5: 1-9.
27. Jones, B. and O'Neill, B.C. (2020) Global one-eighth degree population base year and projection grids based on the Shared Socioeconomic Pathways, Revision 01. NASA Socioeconomic Data and Applications Center (SEDAC).
28. Karra, K., Kontgis, C., Statman-Weil, Z., Mazzariello, J.C., Mathis, M. and Brumby, S.P. (2021) Global land use/land cover with Sentinel-2 and deep learning. In IGARSS 2021, 2021 IEEE International Geoscience and Remote Sensing Symposium (pp. 4704-4707). IEEE.
29. Landis, J.R. and Koch, G.G. (1977) The measurement of observer agreement for categorical data. Biometrics 33: 159-174.
30. Lemos, M.C. and Boyd, E. (2010) The politics of adaptation across scales: The implications of additionality to policy choice and development. In M.R. Redclift and M. Grasso (Eds.), Handbook on climate change and human security (pp. 96-110). Edward Elgar.
31. Lwasa, S. (2010) Adapting urban areas in Africa to climate change: The case of Kampala. Current Opinion in Environmental Sustainability 2: 166-171.
32. Mahapatra, M., Ratheesh, R. and Rajawat, A.S. (2015) Sea level rise and coastal vulnerability assessment for the Bay of Bengal coast of India. Natural Hazards 76: 139-159.
33. Mahmood, R., Ahmed, N., Zhang, L. and Li, G. (2022) Coastal vulnerability assessment of the Niger Delta to sea-level rise using a GIS-based composite index. Estuarine, Coastal and Shelf Science, 270, 107822.
34. Maxwell, A.E., Warner, T.A. and Fang, F. (2018) Implementation of machine-learning classification in remote sensing: An applied review. International Journal of Remote Sensing 39: 2784-2817.
35. Murali, R.M., Ankita, M., Amrita, S. and Vethamony, P. (2013) Coastal vulnerability assessment of Puducherry coast, India, using the analytical hierarchical process. Natural Hazards and Earth System Sciences 13: 3291-3311.
36. Musa, Z.N., Popescu, I. and Mynett, A. (2014) The Niger Delta's vulnerability to river floods due to sea level rise. Natural Hazards and Earth System Sciences 14: 3317-3329.
37. O'Neill, B.C., Kriegler, E., Ebi, K.L., Kemp-Benedict, E., Riahi, K., Rothman, D.S., van Ruijven, B.J., van Vuuren, D.P., Birkmann, J., Kok, K., Levy, M. and Solecki, W. (2017) The roads ahead: Narratives for shared socioeconomic pathways describing world futures in the 21st century. Global Environmental Change 42: 169-180.
38. Pekel, J.-F., Cottam, A., Gorelick, N. and Belward, A.S. (2016) High-resolution mapping of global surface water and its long-term changes. Nature 540: 418-422.
39. Pelling, M. (2003) The vulnerability of cities: Natural disasters and social resilience. Earthscan.
40. Pendleton, E.A., Thieler, E.R. and Williams, S.J. (2010) Importance of coastal change variables in determining vulnerability to sea- and lake-level change. Journal of Coastal Research 26: 176-183.
41. Reichstein, M., Camps-Valls, G., Stevens, B., Jung, M., Denzler, J., Carvalhais, N. and Prabhat (2019) Deep learning and process understanding for data-driven Earth system science. Nature 566: 195-204.
42. Roberts, D.R., Bahn, V., Ciuti, S., Boyce, M.S., Elith, J., Guillera-Arroita, G., Hauenstein, S., Lahoz-Monfort, J.J., Schroeder, B., Thuiller, W., Warton, D.I., Wintle, B.A., Hartig, F. and Dormann, C.F. (2017) Cross-validation strategies for data with temporal, spatial, hierarchical, or phylogenetic structure. Ecography 40: 913-929.
43. Rumelhart, D.E., Hinton, G.E. and Williams, R.J. (1986) Learning representations by back-propagating errors. Nature 323: 533-536.
44. Saaty, T.L. (1980) The analytic hierarchy process: Planning, priority setting, resource allocation. McGraw-Hill.
45. Sirko, W., Brempong, E.A., Marcos, J.T.C., Annkah, A., Korme, A.A., Hassen, M.A., … Quinn, J. (2023) High-resolution building and road detection from Sentinel-2 (arXiv:2310.11622). arXiv.
46. Sirko, W., Kashubin, S., Ritter, M., Annkah, A., Bouchareb, Y.S.E., Dauphin, Y., … Quinn, J. (2021) Continental-scale building detection from high resolution satellite imagery (arXiv:2107.12283). arXiv.

47. Syvitski, J.P.M., Kettner, A.J., Overeem, I., Hutton, E.W.H., Hannon, M.T., Brakenridge, G.R., … Nicholls, R.J. (2009) Sinking deltas due to human activities. Nature Geoscience 2: 681-686.
48. Tehrany, M.S., Jones, S. and Shabani, F. (2019) Identifying the essential flood conditioning factors for flood prone area mapping using machine learning techniques. Catena 175: 174-192.
49. Thieler, E.R. and Hammar-Klose, E.S. (2000) National assessment of coastal vulnerability to sea-level rise: Preliminary results for the U.S. Atlantic Coast (Open-File Report 99-593). U.S. Geological Survey.
50. United Nations Office for Disaster Risk Reduction. (2015) Sendai framework for disaster risk reduction 2015-2030. UNISDR.
51. United Nations Office for Disaster Risk Reduction. (2019) Global assessment report on disaster risk reduction 2019. UNDRR, Geneva.
52. Vitousek, S., Barnard, P.L., Fletcher, C.H., Frazer, N., Erikson, L. and Storlazzi, C.D. (2017) Doubling of coastal flooding frequency within decades due to sea-level rise. Scientific Reports 7: 1399.
53. Wisner, B., Blaikie, P., Cannon, T. and Davis, I. (2004) At risk: Natural hazards, people's vulnerability and disasters (2nd ed.). Routledge.
54. WorldPop. (2018) Global high resolution population denominators project, Nigeria (UN-adjusted, 2020). University of Southampton / WorldPop.